Adsorption of Cr(VI) onto *Elaeagnus* Tree Leaves: Statistical Optimization, Equilibrium Modeling, and Kinetic Studies

Javad Zolgharnein* and Ali Shahmoradi

Department of Chemistry, Faculty of Science, Arak University, 38156-876, Arak, Iran

A 2^{4-1}(IV) half-fractional factorial design was performed to identify significant variables for the biosorption of Cr(VI) by *Elaeagnus* tree leaves. A face-centered central composite design (FCCD) was carried out to find a suitable response surface relating all significant variables to *R* (removal) and *q* (sorption capacity). Simultaneous optimization of both responses (*R* and *q*) was carried out, and 80 % of the goal of desirability function was achieved. Simultaneous optimization of *R* and *q* and simple optimization of *q* was more favorable than that of *R* from an environmental and economical view. A kinetics study was performed by examining pseudofirst-order, second-order, and intraparticle diffusion kinetic models, and the best fit was obtained for the pseudosecond-order kinetics model with q_e = (0.624 and 2.657) mg·g^{-1} for (10 and 50) mg·L^{-1} Cr(VI), respectively. Langmuir, Freundlich, and Dubinin−Radushkevich models were used for the equilibrium study. The equilibrium data had the best fit with the Langmuir isotherm. Biosorption mean free energy (*E*) was calculated to be 16.2 kJ·mol^{-1}. Considering kinetics and equilibrium studies, one can suggest that adsorption onto the sites is the rate-limiting step and that biosorption goes through chemisorption mechanisms. Fourier transform infrared (FTIR) spectra were recorded to identify functional groups involved in the biosorption.

Introduction

Contamination of water resources by heavy metals is of great environmental concern. Traditional methods like precipitation, coagulation, electrolysis, and biological treatment for their removal may not be cost-effective. Making use of resins including Amberlit XAD-1180,[1] Amberlite IRA-400 Cl^- and its hybrids,[2] Lewatit FO36 nano ion-exchange resin,[3] and multiwalled carbon nanotubes[4] and liquid−liquid extraction[5] for chromium removal have also been reported earlier. Recently, application of biosorbent materials was considered as a successful alternative to solve this problem.[6,7] Although most applications of biomass address the removal of metal cations, recently more attention is paid to the uptake of toxic metals in anionic forms. Cr(VI) has high environmental and health risks, including cancer in the digestive tract and lungs, and may cause epigastric pain, nausea, vomiting, severe diarrhea, and hemorrhage. Despite high toxicity, many industrial applications have been found including in dye and pigment production and in the tannery, ink, and aluminum manufacturing industries, and so forth.[8] Cr(VI) is more toxic than Cr(III) because of its carcinogenic and mutagenic effects. Therefore, it is necessary to eliminate Cr(VI) from wastewaters before discharge. Usually, Cr(VI) is present in the form of oxyanions such as $HCrO_4^-$ and $Cr_2O_7^{2-}$ in aqueous solutions, and the relative proportion of each species depends on both pH and Cr(VI) concentration.[8,9] Several biomass materials are used for removing chromium from aqueous waste, but to the best of our knowledge, there is no report about using *Elaeagnus* tree leaves in the literature.[6−13] They are in great supply, inexpensive, and easily available and have no commercial usage. The present study introduces *Elaeagnus* tree leaves as a novel biosorbent for removing chromium(VI) and tries to optimize both the removal efficiency percentage (*R* %) and the biosorption capacity (*q*) simultaneously.[11−13] The contact time (*t*), pH of solution, amount of sorbent (*S*), and initial concentration of Cr(VI) (C_m) were studied as effective variables.[11−13] When the list of influencing variables is being populated, the total number of runs in full-factorial design increases so large as 2^k, which is not desirable.[14−16] Therefore, a lot of time and reagent would be wasted. To overcome this problem, a carefully chosen fraction of the runs specified by the full factorial design was carried out.[14−16] In the case of half-fractional factorial design (2^{k-1}), the total number of runs remarkably decreases, but because of the confounding of the main effects and some interactions with each other, the estimation and interpretation of factor coefficients and their interaction are more complicated. Thus, use of fractional factorial design for screening the variables and interactions on the biosorption process are quite sparse.[17−20]

In this study we have planned to use half-fractional factorial design for the screening of variables and central composite design (CCD) surface methodology for providing a suitable mathematical model.[17−20] Here, response data lead to a nonnormal residual distribution. Therefore, data transformation was performed for *R* % and *q* to solve the problem.[14−16] The adequacy of model was checked by some relevant statistical tests. Simultaneous optimization of both responses was done through Dringers's equation.[13,17] Kinetic and thermodynamic studies were also performed to identify the rate limiting step and the possible mechanism of the biosorption process. It can be based on the following mechanisms: physical adsorption, ion exchange, complexation, and precipitation. Biosorption may not necessarily consist of a single mechanism. In many sorption processes, several mechanisms often act in combination, and it is difficult to distinguish between the single steps.[21−23]

Experimental Section

Biosorbent Materials. *Elaeagnus* tree leaves were collected from a groove in a suburb of Arak, an industrial city in the

* Corresponding author. E-mail: j-zolgharnein@araku.ac.ir.

10.1021/je100157y
Published on Web 06/08/2010

Table 1. Factor Names Together with Their Real and Coded Values

factor	levels −1	0	+1
C_m (metal concentration, mg·L^{-1})	10	30	50
S (sorbent, mg·g^{-1})	0.1	0.2	0.3
pH (initial pH solution)	2	4	6
t (contact time, min)	10	55	100

center of Iran. The leaves were washed with tap water until the supernatant solution become clear and then rinsed using doubly distilled water. They were dried on a clean table at room temperature. The dried leaves were ground and sieved to (40 to 50) mesh and then stored in a plastic bag for further use.

Metal Solution. The stock solution of Cr(VI) was prepared by dissolving appropriate quantities of $K_2Cr_2O_7$ salt in doubly distilled water. HNO_3 and NaOH were used for the pH adjustment of solutions. All of the chemicals were of analytical grade and obtained from Merck (Darmstadt, Germany). Doubly distilled water was used throughout. Ten milliliters of Cr(VI) solution was poured into 100 mL Erlenmeyer flasks. A known amount of dried biomass was added to each sample solution. The pH of solution was adjusted before the addition of biosorbent. Fresh dilutions were made for each study.

Batch Biosorption Procedure and Metal Analysis. Batch experiments were carried out under the following conditions: The biosorbent was suspended in solutions containing Cr(VI) whose concentrations were set according to the experimental design methodology. The dosage of biosorbent was in the range of (0.1 to 0.3) g in the 10 mL solution. The pH, amount of sorbent (S), and initial Cr(VI) concentration (C_m) employed are shown in Table 1. Samples were collected and filtered after 100 min through 0.45 μm Whatman filter paper. The concentration of Cr(VI) remaining in solution after biosorption was determined by using a Perkin-Elmer 2380 atomic absorption spectrophotometer. Instrumental conditions were adjusted as recommended by the manufacturer applying a current of 25.0 mA. The sensitive wavelength for chromium at 357.9 nm was used with a slit bandwidth of 0.7 nm.

The removal percent (R %) and amount of adsorbed Cr(VI) (q) by the biomass from aqueous solution were determined by eqs 1 and 2, respectively.

$$R = 100(C_{mi} - C_{mf})/C_{mi} \quad (1)$$

$$q = (C_{mi} - C_{mf})V/S \quad (2)$$

where C_{mi} (mg·L^{-1}) is the initial concentration, C_{mf} (mg·L^{-1}) the final concentration of the Cr(VI) in the solution, q the amount of Cr(VI) taken up by the biosorbent (mg·g^{-1}), V the volume of solution (L), and S weight of biomass (g) in grams.

FTIR Spectrometry. The FTIR spectra of dried native and metal-loaded biomass in the range of (400 to 4000) cm^{-1} were recorded by using a Unicam-Galaxy series FTIR 5000 to obtain information about the nature of the possible functional groups involved in the biosorption process.

Data Analysis. Biosorption processes were preformed in a batch system. Each variable was tested at three levels, namely, a high level denoted by +1, a medium level (0) and a low level (−1) as listed in Table 1. Optimization was carried out in two steps. First, by using fractional factorial design, the effective variables on biosorption process were identified. Then the identified effective factors were optimized by using face-centered central composite design (FCCD).[24] MINITAB version 15, JMP version 7, SPSS version 15, and MAPLE version 10 were utilized for statistical and mathematical calculations.

Table 2. Design Matrix for 2^{4-1}(IV) Fractional Factorial Design and Experimental Results

std order	run order	center pt	blocks	C_m	S	pH	t	R	q
10	1	0	1	0	0	0	0	62.44	0.94
7	2	1	1	−1	1	1	−1	57.5	0.19
8	3	1	1	1	1	1	1	71.21	1.19
1	4	1	1	−1	−1	−1	−1	58.09	0.58
3	5	1	1	−1	1	−1	1	77.44	0.26
2	6	1	1	1	−1	−1	1	55.84	2.79
9	7	0	1	0	0	0	0	62.5	0.94
6	8	1	1	1	−1	1	−1	33.28	1.66
5	9	1	1	−1	−1	1	1	57.27	0.57
4	10	1	1	1	1	−1	−1	73.1	1.22

Table 3. Estimate of the Effects from the 2^{4-1}(IV) Fractional Factorial Design with the Defining Relation $I = C_m \cdot S \cdot pH \cdot T^a$

	R %			q		
term	effect	coef.	P	effect	coef.	P
constant		60.466	0		1.0581	0
$C_m + S \cdot pH \cdot t$	−4.217	−2.109	0.005	1.3144	0.6572	0
$S + C_m \cdot pH \cdot t$	18.693	9.346	0.001	−0.6887	−0.3443	0
$pH + C_m \cdot S \cdot t$	−11.303	−5.651	0.002	−0.3085	−0.1543	0.001
$t + C_m \cdot S \cdot pH$	9.948	4.974	0.002	0.2887	0.1443	0.001
$C_m \cdot S + pH \cdot t$	8.903	4.451	0.002	−0.3368	−0.1684	0.001
$C_m \cdot pH + S \cdot t$	−0.923	−0.461	0.021	−0.2712	−0.1356	0.001
$C_m \cdot t + S \cdot pH$	0.387	0.194	0.049	0.2596	0.1298	0.001
center pt		2.004	0.011		−0.121	0.003

[a] R % = removal percent, q = capacity uptake.

Nonlinear Regression Analysis. All of the kinetics and equilibrium model parameters were evaluated by nonlinear regression using the SPSS 15 software. To quantitatively compare the applicability of each model, apart from the regression coefficient, a normalized standard deviation Δq is calculated as follows;[22]

$$\Delta q\,\% = \sqrt{\frac{\sum [(q_{e,exp} - q_{e,cal})/q_{e,exp}]^2}{n-1}} \quad (3)$$

where q_e is the sorbent capacity at the equilibrium experimental condition ($q_{e,exp}$) and calculated ($q_{e,cal}$), respectively, and n is the number of data points. Since Δq % represents agreement between the experimental and the predicted data points, it provides a numerical measure to interpret the goodness of fit of a given mathematical model to the data.

Results and Discussion

Optimization Strategy. Screening Important Factors Using Fractional Factorial Design. A 2^{4-1}(IV) fractional factorial design with twice replication of the center point requiring only 10 runs was performed for screening the main factors. The resolution of this design is 4, which prevents the main factors from being aliased with any other main effects as well as two-factor interactions. However, two-factor interactions are aliased with each other.[14−16] The design matrix is shown in Table 2. In most cases, main factor effects are much greater than that of the higher-order alias.[14−16] Here, for example, $C_m + S \cdot pH \cdot t$ confounded effect is effective with $P < 0.05$ (Table 3). This can be attributed to the significance of C_m or $S \cdot pH \cdot t$ or both C_m and $S \cdot pH \cdot t$. Usually the effect of the main factor, here C_m, is so large that it can be considered a significant factor by itself. More experiments are needed to determine whether the $S \cdot pH \cdot t$ effect is also significant or not. In this way, all of the main factors were significant in the range studied. The confounded two-factor interactions are also significant and require further interpretation. Figure 1, parts a and b, illustrates

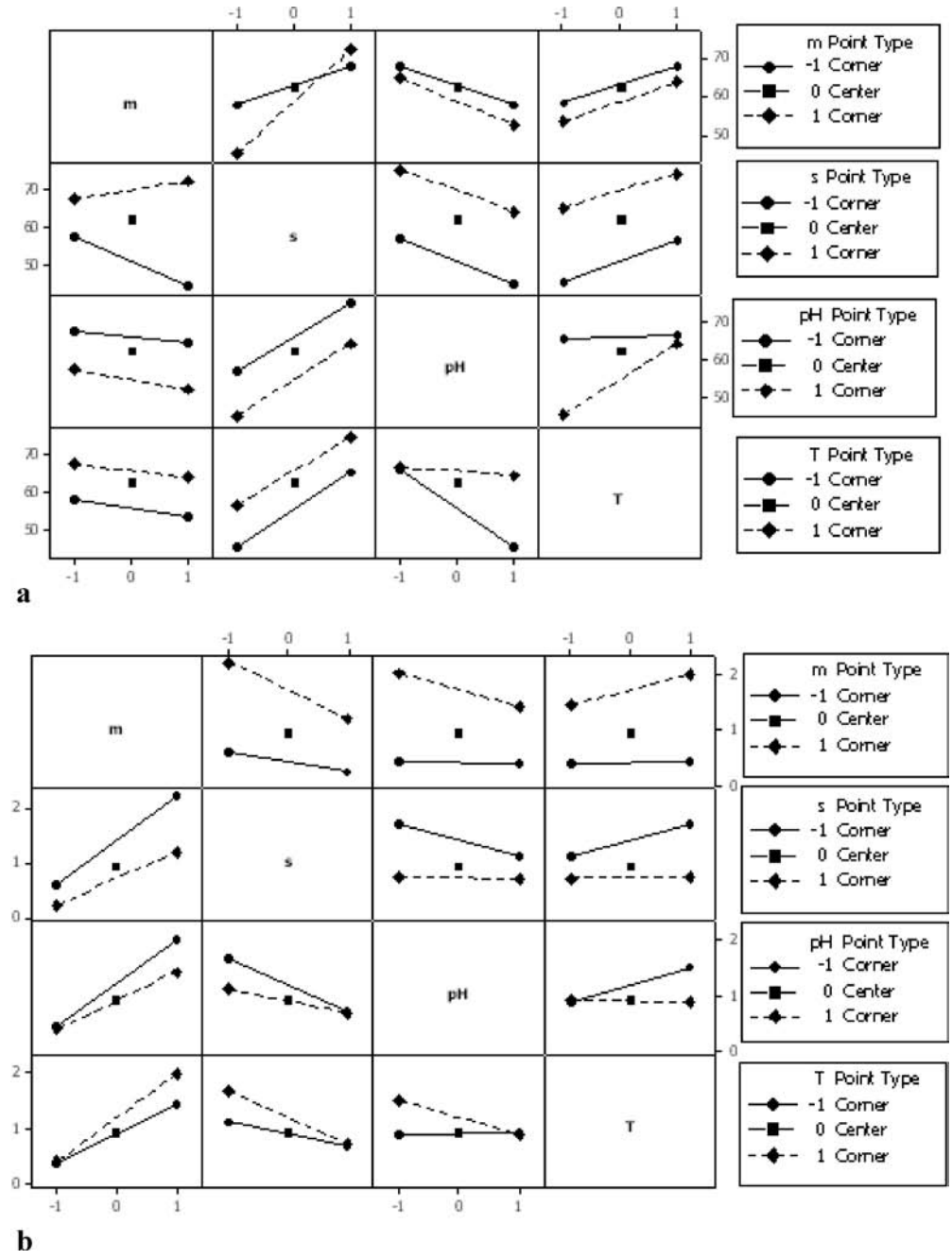

Figure 1. (a,b) Interaction plots of aliased effects for *R* and *q* as responses, respectively.

an interaction plot of factors. Estimated effects are given in Table 3. Referring to Table 3 and Figure 1a,b, it reveals that C_m and pH have a negative effect, but *S* and *t* have a positive effect. In addition, it can be deduced that there is rather a strong interaction between some factors (unparallel interaction line), while the interaction is weaker for some others (parallel interaction line). The negative effect of pH may be explained by that at low pH the surface of the biosorbent will be surrounded by a high quantity of hydronium ions, which will promote the approach of negatively charged $Cr_2O_7^{2-}$.[23] In addition, curvature for the model is significant, and thus we do not expect a planar sheet as a suitable response surface map. Therefore, the identified significant variables ($P < 0.05$), were further optimized according to the FCCD.

Response Surface Methodology. A FCCD[24] was applied as response surface methodology (RSM) to find the optimum levels for effective factors so that maximum biosorption capacity and removal percent were obtained. This design (FCCD) consists of a full factorial or fractional design and also a star design in which experimental points are at a distance α from its center and a center point. The total number of experiments was $N = k^2 + 2k + c_p$, where *k* is number of independent variables and c_p is the replicate number of the central point. The 2*k* denotes the numbers of star points with certain α.[17] Each factor was studied at three levels (−1, 0, 1); in FCCD design, α is equal to ± 1 (Table 4). Literature reviews and our previous experience show that, for Cr(VI) biosorption, 100 min is not long.[25] Considering the positive effect of time, its higher level was used for more optimization, and the remaining three factors were further examined according to the FCCD.

Finding Models. Ordinary least-squares (OLS) assumes that variance distributions of obtained data are normal and homogeneous (homoscedasticity). A model is reliable when it meets these assumptions. In some cases due to uncontrolled factors which

Table 4. FCCD for C_m (Metal Ion Concentration), S (Sorbent Amount), and pH[a]

C_m	S	pH	R	q	log R (exp.)	log q (exp.)	log R (pred.)	log q (pred.)
−1	−1	−1	53.84	0.54	1.731	−0.269	1.731	−0.269
0	0	−1	68.00	1.02	1.833	0.009	1.838	0.014
−1	0	0	72.22	0.36	1.859	−0.442	1.858	−0.442
0	0	1	69.36	1.04	1.841	0.017	1.838	0.014
0	0	0	69.25	1.04	1.840	0.017	1.838	0.014
−1	1	1	75.73	0.25	1.879	−0.598	1.879	−0.598
0	1	0	75.35	0.75	1.877	−0.123	1.880	−0.120
1	1	−1	74.98	1.25	1.875	0.097	1.874	0.096
0	0	0	69.37	1.04	1.841	0.017	1.838	0.014
1	−1	−1	55.83	2.79†	1.747	0.446	1.746	0.445
−1	1	−1	77.87*	0.26	1.891	−0.586	1.891	−0.586
0	0	0	68.62	1.03	1.836	0.013	1.838	0.014
0	0	0	69.10	1.04	1.839	0.016	1.838	0.014
0	−1	0	50.65	1.52	1.705	0.182	1.707	0.183
1	0	0	65.20	1.63	1.814	0.212	1.818	0.216
0	0	0	68.72	1.03	1.837	0.013	1.838	0.014
1	1	1	75.54	1.26	1.878	0.100	1.877	0.099
−1	−1	1	56.82	0.57	1.755	−0.245	1.754	−0.245
1	−1	1	39.57	1.98	1.597	0.296	1.596	0.295
0	0	0	68.85	1.03	1.838	0.014	1.838	0.014

[a] Result of the best condition for achieving maximum q is marked with a dagger (†). Predicted maximum value of R is marked with an asterisk (*).

Table 5. ANOVA Results for Both Suggested Models[a]

Analysis of Variance										
	log R response					log q response				
source	DF	SS	MS	F	P	DF	SS	MS	F	P
regression	8	0.102465	0.012808	1515.75	0.000	9	1.39635	0.15515	17026.44	0.000
residual error	11	0.000093	0.000008			10	0.00009	0.00001		
lack of fit	4	0.000032	0.000008	0.94	0.494	3	0.00003	0.00001	1.18	0.383
pure error	7	0.00006	0.000009			7	0.00006	0.00001		
total	19	0.102558				19	1.39644			

[a] DF = degrees of freedom, SS = sum of squares, MS = mean square, F = F ratio.

affect the response, this may not hold. Data transformation may overcome the problem.[14−16] Here, logarithmic transformation was used to transform the data. Distributions of residuals and correlation between error terms were examined according to Anderson−Darling and Durbin−Watson statistics, respectively.[26,27] Multiple regression analysis was performed to find out a mathematical relation describing R and q as a function of the process variables. The following models were calculated to be suitable regression equations:

$$\log q = 0.0138 + 0.329C_m - 0.152S + 0.0155C_mS - 0.0197C_m \cdot \mathrm{pH} + 0.0147S \cdot \mathrm{pH} + 0.0235C_mS \cdot \mathrm{pH} - 0.127{C_m}^2 + 0.0176S^2 - 0.0169 \cdot \mathrm{pH} \cdot {C_m}^2$$
$$R - Sq(\mathrm{adj}) = 99.8\ \% \qquad R - Sq(\mathrm{pred}) = 98.95\ \%$$
$$\text{Durbin−Watson statistic} = 1.7\ (P = 0.18 > 0.05) \tag{4}$$

and

$$\log R = 1.84 - 0.0203C_m + 0.0866S + 0.0155C_mS - 0.0197C_m \cdot \mathrm{pH} + 0.0147S \cdot \mathrm{pH} + 0.0235C_mS \cdot \mathrm{pH} - 0.0444S^2 - 0.0169 \cdot \mathrm{pH} \cdot {C_m}^2$$
$$R - Sq(\mathrm{adj}) = 100.0\ \% \qquad R - Sq(\mathrm{pred}) = 99.92\ \%$$
$$\text{Durbin−Watson statistic} = 1.62\ (P = 0.17 > 0.05) \tag{5}$$

Table 5 illustrates ANOVA results for the suggested models. As can be seen, these models have been extremely well fit with high $R-Sq$(adj) and nonsignificant lack of fit. The models cannot explain at most 0.1 % of the total variance. Figures 2a,b and 3a,b show that the distribution of residuals is normal ($P > 0.05$) and illustrate that the variances are homogeneous. On the other hand, according to the Durbin−Watson statistic, one fails to detect the presence of autocorrelation in the residuals ($P > 0.05$). Therefore, the assumptions are valid, and the results are reliable.

Model Validation. High values obtained as $R-Sq$(pred) through cross-validation for both models suggest that the models are reliable for prediction. Using the Maple optimization toolbox, one finds a maximum R % in pH = 6, S = 0.3 g, and C_m = 24.1 mg·L^{-1} as (78.34 ± 1.26) % at the 95 % confidence interval. The q value corresponding to this condition is 0.63 mg·g^{-1}. The maximum value of q is (2.75 ± 0.06) mg·g^{-1} at pH = 2, S = 0.1 g, and C_m = 50 mg·L^{-1}, which corresponds to R = 55 %.

The real values were drawn from the relation between coded and real values as the following:

$$X^* = (X - X_c)/D \tag{6}$$

where X^* is the coded value of factor X, X_c is the center point location for factor X, and D is the interval between the experimental units along factor X.

As a typical illustration, Figure 4 shows a three-dimensional representation of log q as a function of two independent variables, while the third is being kept at its founded optimum value.

The maximum removal percent (R %) at optimum conditions through performing experimental runs reached 78 %. It has good agreement with the predicted value. Haphazardly, the result of the best condition for achieving maximum q is previously available in Table 4 (marked with a dagger, †). These show good predictability of both proposed models. Comparing this predicted maximum value of R with that given in Table 4

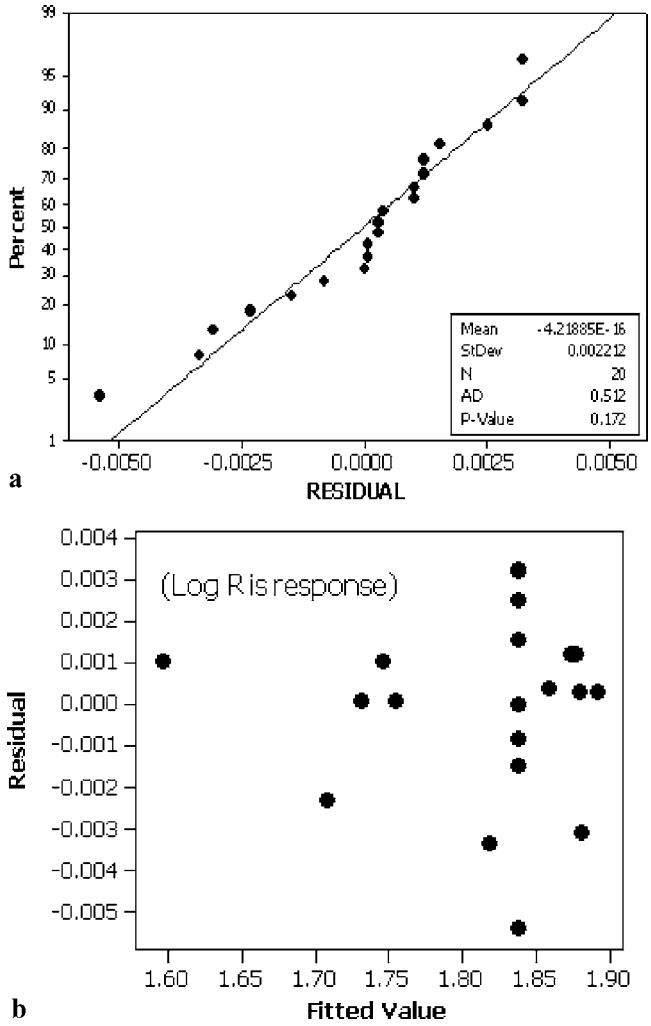

Figure 2. (a,b) Normal probability plot of aliased effects and residuals vs fitted values plot, respectively, with log *R* as response.

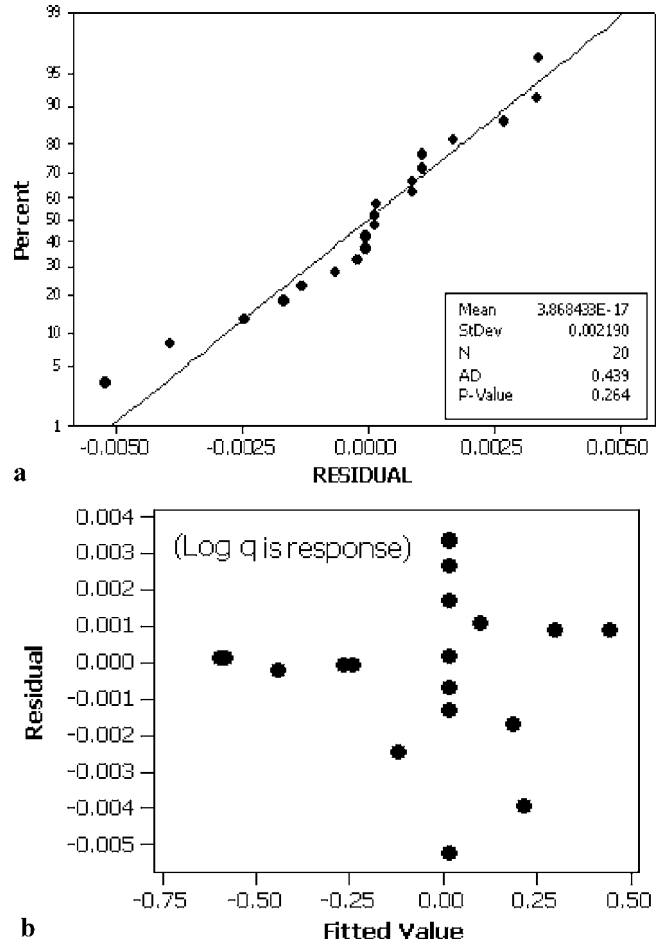

Figure 3. (a,b) Normal probability plot of aliased effects and residuals vs fitted values, respectively, with log *q* as response.

(marked with an asterisk, *) reveals that, despite different experimental conditions, responses are the same statistically. This may be due to the fact that in the concentration range used for Cr(VI), when the sorbent mass is at a high level, it can remove the same amount of metal ion regardless of the initial pH of solution. It may be attributed to a greater effect of *S* relative to C_m and pH so that it can mask the effect of changing C_m and pH (Table 3). This is a very important finding because it makes time-consuming pH and C_m levels preadjustments unnecessary.

Simultaneous Optimization Using the Desirability Function. Separate optimization of *q* and *R* is worthy in its place. Nevertheless, having highest removal efficiency with the least amount of sorbent usage is more favorable, because high removal efficiency guarantees satisfactory decontamination of the solution and high *q* avoids excess waste production. This may be realized through simultaneous maximization of *q* and *R* %. A difficulty arises here, because when conditions are adjusted for increasing *R*, the *q* value drops and vice versa. Therefore, a compromise must be established to ensure having the highest possible values of *q* and *R* at the same time.[13,17] A straightforward approach is to overly counter-plot each response. This method works well when there are only a few responses to optimize. Here, one tries to find a set of conditions that optimizes all responses or keeps them in the desired range. Another useful approach is to convert each response to an individual desirability function and then optimize the overall desirability function by adjusting independent variables. A complete description of the method is given in the literature and thus is not reproduced here.[13,16,17] JMP is a statistical software package capable of simultaneous optimization of multiple responses. It yields $R = 73.2$ % and $q = 1.69$ $mg \cdot g^{-1}$ with 80 % desirability in $C_m = 50$ $mg \cdot L^{-1}$, $S = 0.21$ g, and pH = 2. Figure 5 shows a profile of simultaneous optimization efficiency (*R* %) and the inverse of the adsorbent capacity (*q*).

Economical and Environmental Considerations. To simplify a comparison between the results obtained through separate and simultaneous optimization, the results are summarized in Table 6. It is clear that neither *R* nor *q* is in their previously found maximum, but a compromise has been established. Table 6 gives an interesting result. When only *R* was optimized, a worse result was obtained, since by using 0.3 g of sorbent, only 0.188 mg of metal ion was removed. This is due to the low *q* value, and therefore a little amount of biosorbent capacity is used. It leads to excess waste production, which is feasible neither economically nor environmentally. A comparison between *q* and composite optimization results shows that, by increasing the sorbent mass by 100 % (in the passage from *q* to composite optimization), only 33 % improvement in the mass of removed metal ion results. This seems not to be feasible in the sense of the price that should be paid for increasing the mass of metal ion removal by this amount. Therefore, it appears that optimization of *q* is better than *R* or composite optimization if the method is to be used at a large scale.[7,9]

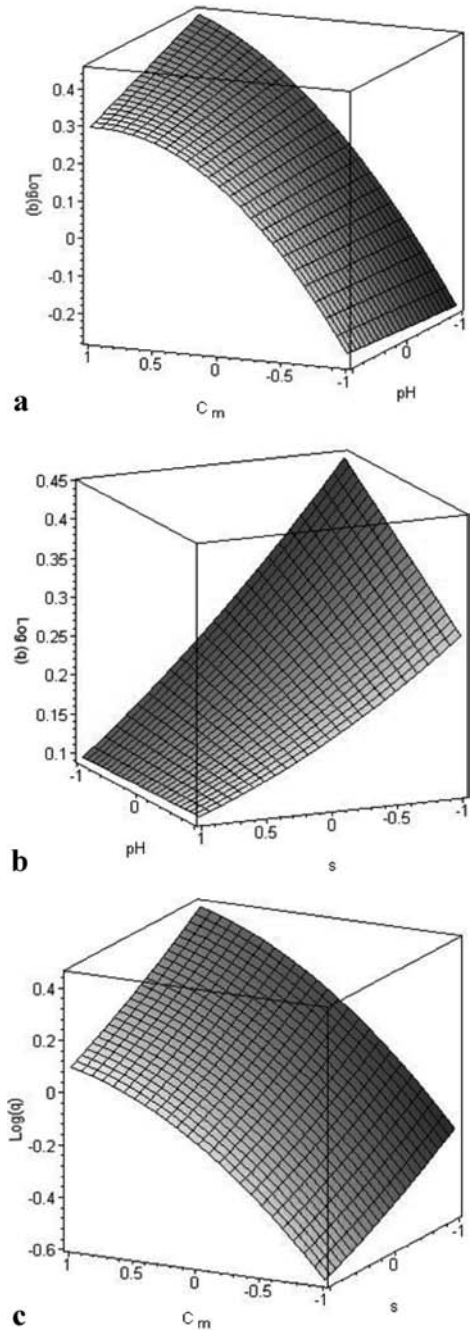

Figure 4. (a) Response surface plot showing the effect of Cr(VI) concentration (C_m) and pH and their mutual effect on log q, while the biomass amount was kept constant at its optimum value. (b) Response surface plot showing the effect on the amount of sorbent (S) and pH and their mutual effect on log q, while the Cr(VI) concentration was kept constant at its optimum value. (c) Response surface plot showing the effect on Cr(VI) concentration (C_m) and amount of sorbent (S) and their mutual effect on log q, while the pH was kept constant at its optimum value.

Biosorption Mechanism. To find the possible mechanism of biosorption, the rate-limiting step, and functional groups involved in the process, equilibrium, kinetics, and FTIR spectroscopy studies were performed.

Equilibrium Modeling. Adsorption isotherms were used to characterize the behavior of metal ion with sorbent. The equation parameters and the underlying thermodynamic assumptions of these equilibrium models often provide some insight into both the sorption mechanism and the surface properties and affinity of the sorbent.[25,28] The Langmuir equation is presented by the following equation:

$$q_e = q_{max}\frac{K_L C_e}{1 + K_L C_e} \tag{7}$$

where K_L is the Langmuir biosorption constant related to the free energy of biosorption. q_{eq} and q_{max} denote the monolayer equilibrium and maximum biosorption capacity, respectively.

The Freundlich model is presented as below

$$q_e = K_F C_e^{1/n} \tag{8}$$

where K_F and n are the Freundlich constants. K_F indicates the relative adsorption capacity of the adsorbent and is related to the bonding energy. The n_F denotes the adsorption intensity. Figure 6 shows that the fit of the data is better for the Langmuir ($R^2 = 0.998$) than the Freundlich isotherm ($R^2 = 0.845$). Therefore, the biosorption process in this study may be interpreted as monolayer adsorption. According to the Langmuir model, sorption occurs uniformly on the active sites of the sorbent, and once a sorbate occupies a site, no further sorption can take place at the site. The fact that the Langmuir isotherm fits the experimental data very well may be due to homogeneous distribution of active sites on the adsorbent surface, since the Langmuir equation assumes that the surface is homogeneous.[25,28,29] The shape of the Langmuir isotherm can be used to predict whether a sorption system is favorable or not in a batch adsorption process. For a Langmuir type biosorption system, a dimensionless factor called separation factor or equilibrium parameter (R_L) is defined as follows:

$$R_L = \frac{1}{1 + K_L C_0} \tag{9}$$

where C_0 is the initial metal ion concentration ($mg \cdot L^{-1}$). The R_L value indicates the type of isotherm.

When $0 < R_L < 1$, the sorption system is favorable.[30,31] This holds when $K_L > 0$. Table 7 shows that the system under study is thermodynamically favorable. The equilibrium data were also subjected to the Dubinin−Radushkevich (D-R) isotherm model to determine the nature of biosorption processes as physical or chemical. The D-R sorption isotherm is more general than the Langmuir isotherm, as its derivation is not based on ideal assumptions such as, equipotent of the sorption sites, the absence of steric hindrance between sorbed and incoming particles and surface homogeneity on the microscopic level.[31]

The D-R isotherm can be written as

$$\ln C_{sorb} = \ln X_m - \beta\varepsilon^2 \tag{10}$$

where C_{sorb} is the amount of Cr(VI) ions sorbed onto the sorbent ($mol \cdot g^{-1}$), X_m represents the maximum sorption capacity of the sorbent ($mol \cdot g^{-1}$), β is a constant related to sorption energy, and ε is the Polanyi sorption potential ($J \cdot mol^{-1}$), the amount of energy required to pull a sorbed molecule from its sorption to infinity, which is equal to

$$\varepsilon = RT\ln\left(1 + \frac{1}{C_e}\right) \tag{11}$$

where R is the gas constant in $kJ \cdot mol^{-1} \cdot K^{-1}$, T the temperature in Kelvin, and C_e the equilibrium concentration in solution ($mol \cdot L^{-1}$). The Polanyi adsorption theory postulates the fixed volume of sorption sites close to the sorbent surface and the existence of sorption potential over these sites. The sorption potential is related to an excess of sorption energy over the condensation energy and is independent of temperature.[31]

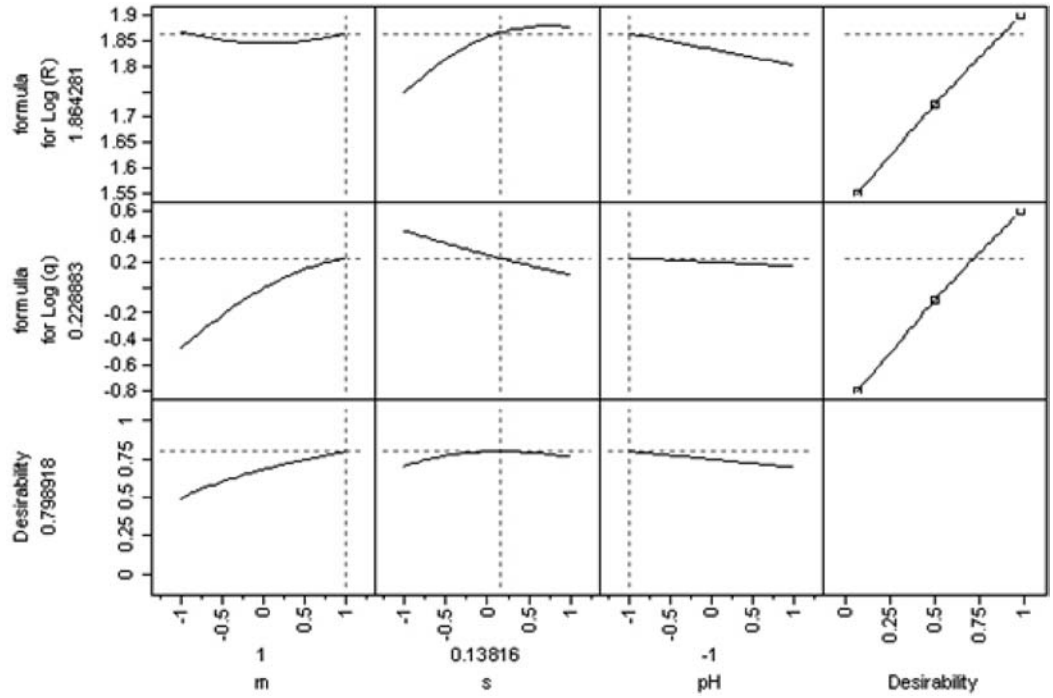

Figure 5. Desirability functions for simultaneous optimization of log R and log q.

Table 6. Comparison between Single and Multiple Optimization of R and q

	single optimization		multiple optimization
	R optimized	q optimized	R and q simultaneously optimized
optimized conditions	$C_m = 24.1$ mg·L^{-1} $S = 0.3$ g pH = 6	$C_m = 50$ mg·L^{-1} $S = 0.1$ g pH = 2	$C_m = 50$ mg·L^{-1} $S = 0.21$ g pH = 2
R % (removal percent)	78 (0.188)[a]	55 (0.275)[a]	73 (0.365)[a]
q (mg·g^{-1})	0.63	2.75	1.69

[a] mg of Cr(VI) removed.

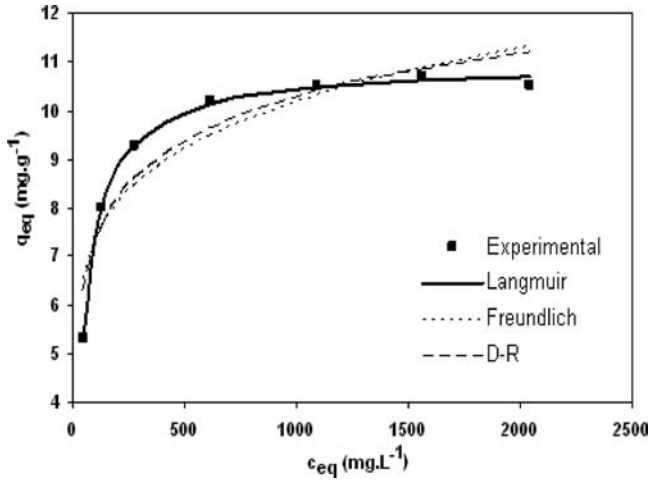

Figure 6. Isotherm study plot in pH = 2, $S = 0.1$ g, and at room temperature.

The essential feature of this isotherm is called the mean free energy of biosorption (E) which is defined as follows

$$E = 1/(2\beta)^{1/2} \quad (12)$$

For an adsorption process with E between (8 and 16) kJ·mol^{-1}, the process is known to follow chemical adsorption ion-exchange, while the process is likely physical adsorption when E is less than 8 kJ·mol^{-1}. Therefore, the adsorption of Cr(VI) in the present study with $E = 16.2$ kJ·mol^{-1} can be considered to be influenced by a chemical ion-exchange mechanism.[29,31,32]

Table 7. Isotherm Parameters of Langmuir, Freundlich, and D-R Models

isotherm	$q_{m,exp}$ / mg·g^{-1}	parameters			
Langmuir		q_m (mg·g^{-1})	K (L·mg^{-1})	R^2	Δq %
	11	10.943	0.02	0.998	0.010
Freundlich		K_F (mg·g^{-1})/(mg·L^{-1})$^{1/n}$	n (L·g^{-1})	R^2	Δq %
	11	3.778	6.968	0.845	0.114
D-R constants		q_m (mg·g^{-1})	β (mol^2·J^{-2})	R^2	Δq %
	11	14.5	$1.9 \cdot 10^{-9}$	0.896	0.092

The constant parameters and coefficient of determination (R^2) are summarized in Table 7. As can be seen from the coefficient of determination (R^2), the Langmuir isotherm is more favorable than the Freundlich isotherm and D-R for the adsorption process of Cr(VI) onto *Elaeagnus* tree leaves. The fact that the Langmuir isotherm fits the experimental data very well ($R^2 = 0.998$) may be due to homogeneous distribution of active sites on the adsorbent surface, since the Langmuir equation assumes that the surface is homogeneous.[30]

Kinetics of Biosorption Process. Dynamics of the adsorption process in terms of the order and the rate constant can be evaluated using kinetics adsorption data. Assuming that the mechanical agitation rate is fast enough, then all of the solute ions can reach the vicinity of sorbent at a sufficient rate, and this step cannot be the rate-determining step (RDS) of the biosorption process. Thus, we should seek RDS in another phenomena occurring during the biosorption process including

(1) diffusion through the boundary layer to the surface of the adsorbent (external diffusion), (2) sorption of ions onto sites, and (3) intraparticle diffusion into the interior of the adsorbent.[33]

It is usually observed that intraparticle diffusion is the rate-determining step, and this usually can be tested using the equation described by the intraparticle model:[33]

$$q_t = K_p t^{1/2} + C \tag{13}$$

where q_t ($mg \cdot g^{-1}$) is the amount adsorbed at time t, K_p is the intraparticle rate constant ($mg \cdot g^{-1} \cdot min^{-1/2}$), and C is a constant. Figure 7 shows this model plots for (10 and 50) $mg \cdot L^{-1}$ Cr(VI) concentrations. Such plots may present a multilinearity,[33] indicating that two or more steps take place. The first, due to fast kinetics of the external surface or instantaneous adsorption stage, is a sharper portion and is absent in the plot. The second is the gradual adsorption stage, where intraparticle diffusion is rate-controlled. The third is the final equilibrium stage where intraparticle diffusion starts to slow down due to low sorbate concentrations in the solution. The stage of intraparticle diffusion control starts and continues from (10 to 50) min. Finally, final equilibrium adsorption starts after 50 min. Cr(VI) is slowly transported via intraparticle diffusion into the particles and is finally retained in the micropores. In general, the slope of the line in stage 2 is called as intraparticle diffusion rate constant, K_p. The rate constant for intraparticle diffusion increased from 0.04 to 0.15 with increasing Cr(VI) concentration from (10 to 50) $mg \cdot L^{-1}$. The higher slope means higher K_p and faster intraparticle diffusion. In addition, the results indicate that the intraparticle diffusion model fits the experimental data well for an initial period of the biosorption processes. In addition the line did not pass through the origin. Therefore, it could be suggested that the mechanism of biosorption was complex and external and intraparticle diffusion contributes to the actual biosorption process.[33,34]

In many cases, the kinetics of adsorption by any biological material has been tested for the first-order expression given by Lagergren.[35] However, it has also been shown that a pseudo-second-order approach can sometimes provide a better description of the adsorption kinetics.

The Lagergren pseudofirst-order model has the following form

$$q_t = q_e[1 + \exp(-k_1 t)] \tag{14}$$

where q_e and q_t are sorbent capacities at equilibrium and time t, respectively. They are in terms of $mg \cdot g^{-1}$, and k_1 is the rate constant of first-order biosorption (min^{-1}).

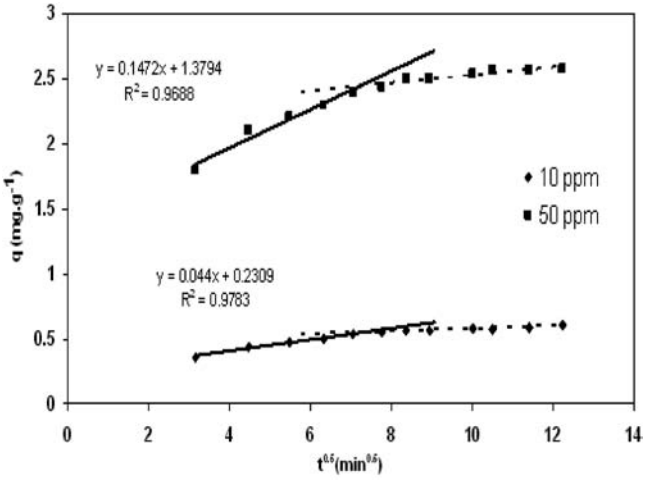

Figure 7. Intraparticle diffusion model plot for (10 and 50) $mg \cdot L^{-1}$ Cr(VI) initial concentration conditions as in Figure 6.

This model assumes that one Cr(VI) ion only sorbs onto one sorption site of the sorbent surface (Cr(VI) in the pH range 1 to 6 which exists in the forms $HCrO_4^-$ and $Cr_2O_7^{2-}$)[9] and is represented by the following scheme:[35]

$$S(solid) + Cr(VI)_{aqueous} \rightarrow S\,Cr(VI)_{(adsorbedphase)} \tag{15}$$

where S is the biosorption site.

The pseudosecond-order model can be written in its nonlinear form as

$$q_t = \frac{k_2 q_e^{\,2} t}{(1 + k_2 q_e t)} \tag{16}$$

The essential assumption of the pseudosecond-order model is that one metal ion is adsorbed onto two surface sites, as indicated by the following equation:[34]

$$2S(solid) + Cr(VI)_{aqueous} \rightarrow S_2Cr(VI)_{(adsorbedphase)} \tag{17}$$

Figure 8 parts a and b shows the fitting of various kinetics models to the experimental data for (10 and 50) $mg \cdot L^{-1}$ Cr(VI). As can be seen, the pseudosecond-order equation provides the best correlation for all of the biosorption data, whereas the

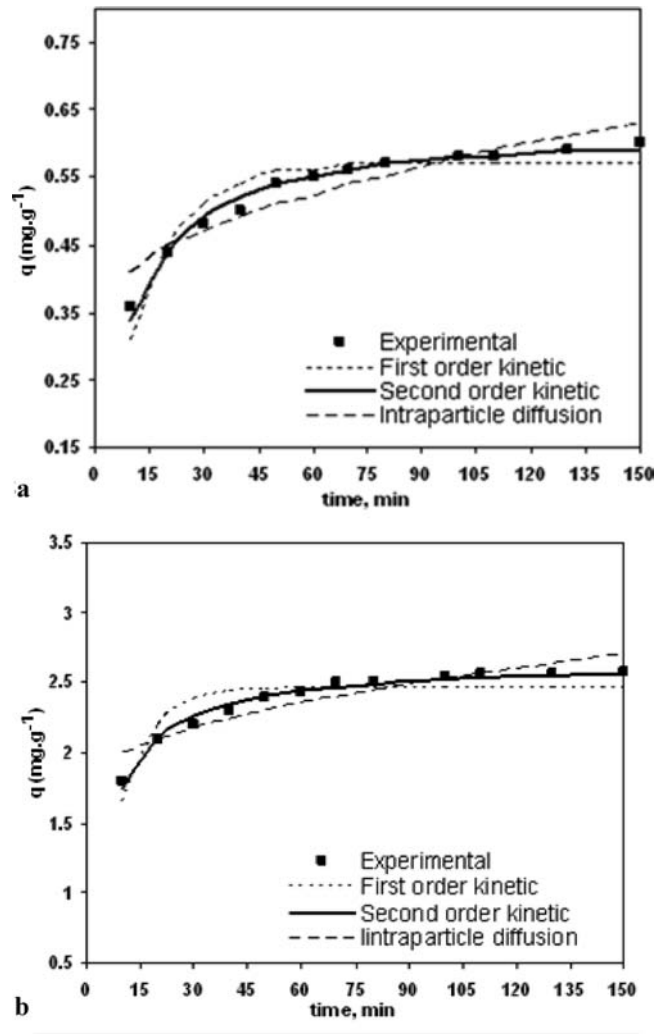

Figure 8. Pseudofirst-order, pseudosecond-order, and intraparticle diffusion kinetics models for (a) 10 $mg \cdot L^{-1}$ and (b) 50 $mg \cdot L^{-1}$ Cr(VI) initial concentrations, respectively, with conditions as in Figure 6.

Table 8. Parameters of Intraparticle Diffusion and First- and Second-Order Kinetics Models

kinetics models	initial concentration / mg·L^{-1}	$q_{e,exp}$ / mg·g^{-1}	parameters			
Pseudofirst Order			K_1 (L·min^{-1})	q_{eq} (mg·g^{-1})	R^2	Δq %
	10	0.6	0.079	0.567	0.859	1.044
	50	2.6	0.11	2.474	0.797	0.049
Pseudosecond Order			K_2 (L·min^{-1})	q_{eq} (mg·g^{-1})	R^2	Δq %
	10	0.6	0.197	0.624	0.985	0.022
	50	2.6	0.072	2.637	0.981	0.015
Intraparticle Diffusion			K_p	c	R^2	Δq %
	10	0.6	0.024	0.338	0.873	0.055
	50	2.6	0.078	0.853	0.853	0.044

pseudofirst-order equation and the intraparticle equation do not give a good fit to the whole experimental data (Table 8). The high Δq % values obtained for the pseudofirst-order model indicate that sorption is not occurring exclusively onto one site per ion. In accordance with the pseudosecond-order reaction mechanism, the overall rate of Cr(VI) sorption processes appears to be controlled by chemical processes, through sharing of electrons between biosorbent and sorbate or covalent forces, through the exchange of electrons between the particles involved.[35,36] Although consistency is expected for these values when the model assumes a single controlling mechanism, variations do occur for natural biosorbents and are usually attributed to the heterogeneous nature of the biosorbent surface. The metal ions may be adsorbed at variable rates by different functional groups at the surface.[30,35,37] The high Δq % values obtained for the intraparticle diffusion model indicate that adsorption is not occurring in the pores of the biosorbent in accordance with surface adsorption. In addition, distinct ionic species might be present simultaneously in the solution; hence, each of them being adsorbed at variable rates as a function of their affinity to the individual functional groups and of the type of binding mechanism has taken place.[37]

FTIR Study. The FTIR analysis of dried *Elaeagnus* tree leaves before and after Cr(VI) adsorption is given in Figure 9. Assignments of spectra in Figure 9 are listed in Table 9. Analysis of the FTIR spectrum after Cr(VI) adsorption showed that there was some shift in the adsorption wavenumber of some peaks, and this indicated that they played a major role in the Cr(VI) biosorption process.[25]

Table 9. FTIR Spectra Assignment for *Elaeagnus* Tree Leaves before and after Uptaking Cr(VI)

IR peak	adsorption bands (C_m^{-1}) sorbent	loaded sorbent	differences	assignment
1	3414.22	3414.22	0	bonded —OH groups, —NH stretching
2	2926.2	2930.06	−3.86	aliphatic C—H group
3	1734.12	1734.12	0	C═O
3	1649.24	1647.31	1.93	C═O
4	1448.63	1437.06	11.57	CH_2 bending
5	1375.33	1375.33	0	CH_3 stretching
6	1319.33	1319.33	0	C—O—C
7	1234.52	1244.16	−9.64	CN stretching
8	1165.08	1161.22	3.86	C—O
9	1051.27	1057.06	−5.79	C—O

Conclusion

Elaeagnus tree leaves were introduced as an abundant and low cost biosorbent of Cr(VI) from aqueous solutions. Its potential adsorption efficiency was considered. Fractional factorial design and FCCD were successfully utilized as statistical optimization strategy. The q optimization was proved to be more economically and environment friendly than R, and also, simultaneous optimization of R and q was performed. Kinetic and equilibrium studies suggested that the predominant mech-

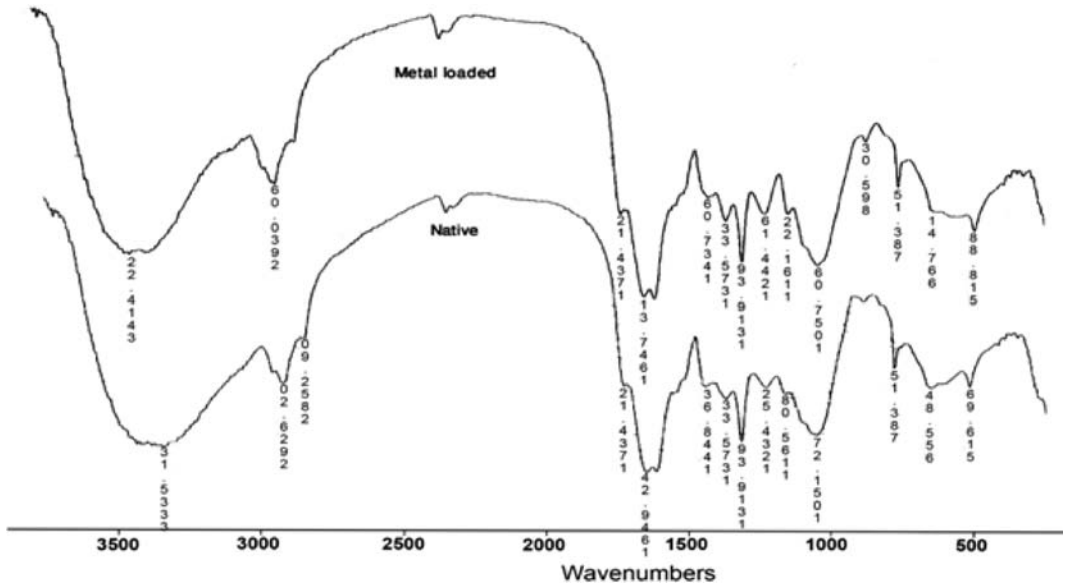

Figure 9. FTIR analysis of the native and Cr(VI) loaded biosorbent.

anism of biosorption of Cr(VI) by *Elaeagnus* tree leaves is chemisorption and the process is thermodynamically favorable.

Literature Cited

(1) Narin, I.; Kars, A.; Soylak, M. A novel solid phase extraction procedure on Amberlite XAD-1180 for speciation of Cr(III), Cr(VI) and total chromium in environmental and pharmaceutical samples. *J. Hazard. Mater.* **2008**, *150*, 453–458.

(2) Syed, M.; Tauqeer, A.; Abdul, N.; Khizar, H. S.; Muhammad, W. Kinetics of chromium ion removal from tannery wastes using Amberlite IRA-400 Cl−and its hybrids. *Water, Air, Soil Pollut.* **2010**; DOI 10.1007/s11270-009-0221-7.

(3) Rafati, L.; Mahvi, A.; Asgari, H.; Hosseini, R. S. Removal of chromium (VI) from aqueous solutions using Lewatit FO36 nano ion exchange resin. *Int. J. Environ. Sci. Technol.* **2010**, *7*, 147–156.

(4) Tuzen, M.; Soylak, M. Multiwalled carbon nanotubes for speciation of chromium in environmental samples. *J. Hazard. Mater.* **2007**, *147*, 219–225.

(5) Kalidhasan, S.; Rajesh, N. Simple and selective extraction process for chromium(VI) in industrial wastewater. *J. Hazard. Mater.* **2009**, *170*, 1079–1085.

(6) Volesky, B. Detoxification of metal-bearing effluents: biosorption for the next century. *Hydrometallurgy* **2001**, *59*, 203–216.

(7) Volskey. B. *Sorption and Biosorption*; BV Sorbex, Inc.: Montreal, Canada, 2003.

(8) Gupta, V. K.; Shrivastava, A. K.; Jain, N. Biosorption of chromium(VI) from aqueous solutions by green algae spirogyra species. *Water Res.* **2001**, *35*, 4079–4085.

(9) Mohan, D.; Pittman, C. U., Jr. Activated carbons and low cost adsorbents for remediation of tri and hexavalent chromium from water. *J. Hazard. Mater.* **2006**, *B137*, 762–811.

(10) Kotas, J.; Stasicka, Z. Chromium occurrence in the environment and methods of its speciation. *Environ. Pollut.* **2000**, *107*, 263–283.

(11) Sangi, M. R.; Shahmoradi, A.; Zolgharnein, J.; Azimi, G.; Ghorbandoost, M. Removal and recovery of heavy metals from aqueous solution using *Ulmus carpinifolia* and *Fraxinus excelsior* tree leaves. *J. Hazard. Mater.* **2008**, *155*, 513–522.

(12) Zolgharnein, J.; Shamoradi, A.; Sangi, M. R. Optimization of Pb(II) biosorption by *Robinia* tree leaves using statistical design of experiments. *Talanta* **2008**, *76*, 528–532.

(13) Zolgharnein, J.; Adhami, Z.; Shahmoradi, A.; Mousavi, S. N. Optimization of removal of methylene blue by *Platanus* tree leaves using response surface methodology. *Anal. Sci.* **2010**, *26*, 111–116.

(14) Massart, D. L.; Vandeginste, B. G. M.; Buydens, L. M. C.; Jong, S. D. E.; Lewi, P. J.; Smeyers Verbeke, J. *Handbook of chemometrics and qualimetrics*, Part A; Elsevier: Amsterdam, 2003.

(15) Bruns, R. E.; Scarmino, I. S.; de Barros Neto, B. *Statistical design-Chemometrics*, 1st ed.; Elsevier: Amsterdam, 2006.

(16) Montgomery, D. C. *Design and analysis of experiments*, 5th ed.; Wiley: New York, 2001.

(17) Bezerra, M. A.; Santelli, R. E. E.; Oliveira, P.; Villar, L. S.; Esclaleira, L. A. Response surface methodology (RSM) as a tool for optimization in analytical chemistry-review. *Talanta* **2008**, *76*, 965–977.

(18) Ferreira, S. L. C.; Bruns, R. E.; Ferreira, H. S.; Matos, G. D.; David, J. M.; Brandao, G. C.; da Silva, E. G. P.; Portugal, L. A.; dos Reis, P. S.; Souza, A. S.; dos Santos, W. N. L. Box-Behnken design: An alternative for optimization of analytical methods. *Anal. Chim. Acta* **2007**, *597*, 179–186.

(19) Pavan, F. A.; Gushikem, Y.; Mazzocato, A. C.; Dias, S. L. P.; Lima, E. C. Statistical design of experiments as a tool for optimizing the batch conditions to methylene blue biosorption on yellow passion fruit and mandarin peels. *Dyes Pigm.* **2007**, *72*, 256–266.

(20) Ferreira, S. L. C.; dos Santoz, W. N. L.; Quintella, C. M.; Neto, B. B.; Bosque-Sandra, J. A. Doehlert matrix: a chemometrics tool for analytical chemistry-review. *Talanta* **2004**, *63*, 1061–1067.

(21) Lacher, C.; Smith, R. W. Sorption of Hg(II) by Potamogeton natans dead biomass. *Miner. Eng.* **2002**, *15*, 187–191.

(22) Wu, F.-C.; Tseng, R.-L.; Juang, R.-S. Kinetic modeling of liquid-phase adsorption of reactive dyes and metal ions on chitosan. *Water Res.* **2001**, *35*, 613–618.

(23) Park, D.; Yun, Y.-S.; Park, J. M. Studies on hexavalent chromium biosorption by chemically-treated biomass of *Ecklonia sp*. *Chemosphere* **2005**, *60*, 1356–1364.

(24) Beg, Q. K.; Sahai, V.; Gupta, R. Statistical media optimization and alkaline protease production from Bacillus mojavensis in a bioreactor. *Process Biochem.* **2003**, *39*, 203–209.

(25) Sari, A.; Tuzen, M. Biosorption of total chromium from aqueous solution by red algae (*Ceramium virgatum*): Equilibrium, kinetic and thermodynamic studies. *J. Hazard. Mater.* **2008**, *160*, 349–355.

(26) Anderson, R. L. *Practical Statistics for Analytical Chemists*; Van Nostrand Reinhold: New York, 1987.

(27) Tabachnik, B. G.; Fidell, L. S. *Experimental designs using ANOVA*; Thomson Learning Academic Resource Center: London, 2007.

(28) Ho, Y. S.; Porter, J. F.; Mckay, G. Equilibrium isotherm studies for the sorption of divalent metal ions onto peat: copper, nickel and lead single component systems. *Water, Air, Soil Pollut.* **2002**, *141*, 1–33.

(29) Sharma, Y. C.; Uma. Optimization of parameters for adsorption of methylene blue on a low-cost activated carbon. *J. Chem. Eng. Data* **2010**, *55*, 435–439.

(30) Dundar, M.; Nuhoglu, C.; Nuhoglu, Y. Biosorption of Cu(II) ions onto the litter of natural trembling poplar forest. *J. Hazard. Mater.* **2008**, *151*, 86–95.

(31) Malik, R.; Hasany, S. M.; Subhani, M. S. Sorptive potential of sun flower stem for Cr(III) ions from aqueous solutions and its kinetic and thermodynamic profile. *Talanta* **2005**, *66*, 166–173.

(32) Özcan, A.; Öncü, E. M.; Özcan, A. S. Kinetics, isotherm and thermodynamic studies of adsorption of Acid Blue 193 from aqueous solutions onto natural sepiolite. *J. Colloid Interface Sci. A* **2006**, *277*, 90–97.

(33) Basha, S.; Murthy, Z. V. P.; Jha, B. Sorption of Hg(II) onto *Carica papaya*: Experimental studies and design of batch sorber. *Chem. Eng. J.* **2008**, *147*, 226–234.

(34) Cheung, C. W.; Porte, J. F.; Mckay, G. Sorption kinetic analysis for the removal of cadmium ions from effluents using bone char. *Water Res.* **2001**, *35*, 605–612.

(35) Ho, Y. S.; McKay, G. The kinetics of sorption of divalent metal ions onto sphagnum moss peat. *Water Res.* **2000**, *34*, 735–742.

(36) Lu, S.; Gibb, S. W. Copper removal from wastewater using spent-grain as biosorbent. *Bioresour. Technol.* **2008**, *99*, 1509–1517.

(37) Oliveira, W. E.; Franca, A. S.; Oliveira, L. S.; Rocha, S. D. Untreated coffee husks as biosorbents for the removal of heavy metals from aqueous solutions. *J. Hazard. Mater.* **2008**, *152*, 1073–1081.

Received for review February 11, 2010. Accepted May 23, 2010.

JE100157Y